Nonlinear Processes in Geophysics (2000) 7: 151–158

Nonlinear Processes in Geophysics

3D reconnection due to oblique modes: a simulation of Harris current sheets

G. Lapenta[1,2] and J. U. Brackbill[2]

[1]Istituto Nazionale per la Fisica della Materia and Dipartimento di Energetica, Politecnico di Torino, Corso Duca degli Abruzzi 24, 10129 Torino, Italy
[2]Los Alamos National Laboratory, Los Alamos, NM 87544, USA

Received: 26 October 1999 – Revised: 25 January 2000 – Accepted: 17 February 2000

Abstract. Simulations in three dimensions of a Harris current sheet with mass ratio, $m_i/m_e = 180$, and current sheet thickness, $\rho_i/L = 0.5$, suggest the existence of a linearly unstable oblique mode, which is independent from either the drift-kink or the tearing instability. The new oblique mode causes reconnection independently from the tearing mode. During the initial linear stage, the system is unstable to the tearing mode and the drift kink mode, with growth rates that are accurately described by existing linear theories. However, oblique modes are also linearly unstable, but with smaller growth rates than either the tearing or the drift-kink mode. The non-linear stage is first reached by the drift-kink mode, which alters the initial equilibrium and leads to a change in the growth rates of the tearing and oblique modes. In the nonlinear stage, the resulting changes in magnetic topology are incompatible with a pure tearing mode. The oblique mode is shown to introduce a helical structure into the magnetic field lines.

1 Introduction

As is well-known, electron compressibility stabilizes the tearing mode in magnetic field structures, like the magnetotail, that have a perpendicular field component across the neutral sheet (Quest *et al.*, 1996). In fact, a recent paper suggests that the conventional model for substorm onset involving reconnection due to the collisionless tearing instability now appears to be untenable because of this stabilization (Wu *et al.*, 1998). However, simulation results appear to contradict this conclusion. The simulations show that reconnection proceeds even in the presence of a perpendicular magnetic field (Pritchett *et al.*, 1996), and that the drift-kink instability is somehow involved. It is important to understand how the kink instability and reconnection are related, if one is to understand the role of collisionless tearing in reconnection in the magnetotail.

Correspondence to: Lapenta

The drift-kink instability is observed in plasma simulations by several groups (Ozaki *et al.*, 1996; Pritchett and Coroniti, 1996; Zhu and Winglee, 1996). Current understanding of the instability rests on the results of these simulations, on two-fluid theories for the drift kink mode developed by Pritchett *et al.*(1996) and Yoon *et al.*(1998) and on kinetic theories developed by Lapenta and Brackbill (1997) and Daughton (1998). Sausage-like modes have also been observed by Büchner *et al.*(1999) in accordance with the kinetic theory by Lapenta and Brackbill (1997) and with the fluid theory by Yoon *et al.*(1998). There are unresolved differences between the simulation results and theoretical predictions. There is, however, general agreement that the drift-kink mode causes a long-wavelength rippling or kinking of the current sheet with a wave vector in the general direction of the current flow, has growth rates on the ion cyclotron time scale and real frequencies on the order of the drift frequency, and may be unstable under conditions that are observed in the magnetotail.

It is important to understand how the drift kink instability acts to allow reconnection to proceed even when there is a perpendicular field. Analysis of electron compressibility must include variation in the direction of current flow, if it is to shed light on the effect of the drift-kink instability on reconnection in three dimensions. Pritchett (Pritchett, 1997) comments that the results of 3-D electromagnetic plasma simulations indicate that this mode can act as a precursor to the growth of tearing modes and subsequent reconnection, and elsewhere that the growth of the kink mode reduces the electron compressibility effect by moving the plasma across flux tubes, which then allows tearing to occur at the underlying 1-D neutral sheet rate (Pritchett and Coroniti, 1996). There is evidence in Pritchett's results for a long latent period before reconnection begins (Pritchett, 1997). However, the nature of the nonlinear interaction between the drift kink instability and the tearing instability is still unresolved. It is to contribute to the resolution of this question that the present study is undertaken.

In unpublished simulations in three dimensions with CE-

LESTE3D at higher electron/ion mass ratios, reconnection is observed to occur in two-dimensional equilibria that are stable to the tearing instability in simulations in two dimensions (Lapenta and Brackbill, 1997b). However, there is some indication that the pure tearing mode is not responsible for the observed reconnection. To understand better the mechanism by which reconnection occurs in such cases, it is argued that a re-examination of the stability of the 1D Harris equilibrium in three dimensions with no perpendicular field can be useful, especially at higher ion/electron mass ratios. First, Fourier analysis in both the kink and tearing directions is meaningful in such cases, the results can be compared directly to linear theory, and oblique modes can be compared directly with those in the principal directions. Second, stabilization of the tearing mode by electron adiabaticity is eliminated, and reconnection rates in 2D and 3D calculations can be compared directly. Third, simulations show that the growth rate of tearing relative to the drift kink mode is smaller as the mass ratio and current sheet thickness increase. Thus, although one is not comparing stable and unstable cases, there is a distinct separation of timescales. It is important to note that in simulations with low mass ratios and thinner current sheets, the relationship between the time scales can be reversed. In particular, for a Harris equilibrium at a mass ratio of $m_i/m_e = 16$, as used in Pritchett *et al.*(1996) the growth rate of the pure tearing mode is faster than that of the kink mode (Lapenta and Brackbill, 1997). For $m_i/m_e = 180$ and $\rho_i/L = 0.5$, where L is the current layer thickness, the drift-kink instability has the higher growth rate. It must be noted that the scaling with the mass ratio of the drift-kink and tearing mode described above is supported by independent simulations (Lapenta and Brackbill, 1997; Ozaki *et al.*, 1996; Horiuchi and Sato, 1999) as well as by some kinetic and fluid theories (Lapenta and Brackbill, 1997; Yoon *et al.*, 1998), but it disagrees with the linear theory by Daughton (1998).

Results for the Harris equilibrium reported here with more realistic mass ratios suggest that an oblique, three-dimensional mode explicitly noted by Pritchett and Coroniti (1996), and suggested by the helical field structures displayed by Zhu and Winglee (1996), directly causes reconnection in three dimensions.

2 Numerical Simulation of the Harris Equilibrium

We consider the time evolution of a plasma initially in a Harris equilibrium. The Harris equilibrium is characterized by the following particle distribution function for species s

$$f_{0s} = n(z)\left(\frac{m_s}{2\pi k T_s}\right)^{3/2} \cdot e^{-\frac{m_s}{2kT_s}\left[v_x^2+(v_y-u_s)^2+v_z^2\right]} \tag{1}$$

The initial magnetic field $\mathbf{B_0}$ is aligned with the x axis. The initial current $\mathbf{J_0}$ is aligned with the y axis. Gradients of the current and magnetic field are aligned with the z axis. The plasma density is given by

$$n(z) = n_s \mathrm{sech}^2(z/L) \tag{2}$$

where L is the width of the current sheet. The magnetic field varies in z as

$$B_x = B_o \tanh(z/L) \tag{3}$$

In the simulations reported here, we choose $m_i/m_e = 180$, $T_i/T_e = 2$, $\omega_{ci}/\omega_{pi} = .0183$ and $\rho_i/L = u_i/2v_{th,i} = 0.5$ where ρ_i is the ion gyroradius. We assume also that the plasma is non relativistic $v_{th,e}/c = 0.1$.

The Harris equilibrium is simulated with the implicit particle in cell code CELESTE3D, which solves the full Vlasov-Maxwell set of equations using the implicit moment method (Brackbill and Forslund, 1985). The Maxwell's equations are discretized in time implicitly:

$$\begin{cases} \epsilon_0 \nabla \cdot \mathbf{E}^1 = n^1 \\ \nabla \times \mathbf{E}^1 = -\dfrac{\mathbf{B}^1 - \mathbf{B}^0}{\Delta t} \\ \nabla \cdot \mathbf{B}^1 = 0 \\ \nabla \times \mathbf{B}^\theta = \epsilon_0 \mu_0 \dfrac{\mathbf{E}^1 - \mathbf{E}^0}{\Delta t} + \mu_0 \mathbf{J}^{1/2} \end{cases} \tag{4}$$

where the new (old) time level is labeled 1 (0). The equations of motion for the computational particles are also discretized implicitly:

$$\begin{cases} \mathbf{x}_p^1 = \mathbf{x}_p^0 + \mathbf{u}_p^{1/2}\Delta t \\ \mathbf{u}_p^1 = \mathbf{u}_p^0 + \dfrac{q_s}{m_s}\left[\mathbf{E}^1 + \mathbf{u}_p^{1/2} \times \mathbf{B}^0\right]\Delta t \end{cases} \tag{5}$$

where the intermediate time level is labeled 1/2. Details of the implicit particle in cell method can be found in the literature (Brackbill and Forslund, 1985).

The implicit formulation makes it possible to simulate phenomena on the ion time scale while retaining electron kinetic contributions. The implicit formulation of the Maxwell's equations removes the speed of light time step limitation, $\Delta t < \Delta x/c$ (Brackbill, 1990). And the implicit formulation of the particle equations of motion removes the plasma frequency time step constraint, $\Delta t < 2/\omega_{pe}$. The simulations described below use $\omega_{pi}\Delta t = 1$, corresponding to $\omega_{pe}\Delta t \sim 13.4$, i.e., to a time step 134 times larger than typical in explicit codes. Further reduction of the cost of three-dimensional simulations results because the implicit formulation allows one to use coarser grids, if one needs only to resolve long wavelength phenomena, than are permitted with explicit codes. The explicit stability conditions on the time step above are replaced by an accuracy condition on the implicit time step, $v_{\mathrm{thermal}}\Delta t < \Delta x$. When one can satisfy this constraint with $\omega_{pe}\Delta t >> 1$, the Debye length can be much smaller than the mesh spacing, $\lambda_{\mathrm{Debye}} << \Delta x$. By comparison, an explicit calculation typically requires that the Debye length be comparable to the mesh spacing to avoid the finite grid instability. Compared with earlier explicit calculations, the implicit calculations reported here use 1/50 the number of cells (Pritchett *et al.*, 1996). Thus, despite the significantly greater cost and complexity of each time step in the implicit formulation, implicit plasma simulations can be an efficient

tool for the study of low frequency, long wavelength phenomena.

The implicit equations give approximately quasi-neutral solutions when the the time step is large compared with the electron plasma frequency and the mesh spacing is large compared with the electron Debye length (Brackbill and Forslund, 1985). In one dimension using CELEST1D (Vu and Brackbill, 1992), some cooling of the electrons and a tendency for ion and electron temperatures to equilibrate was noted with very large time steps. This tendency is reduced if the number of electron particles is increased. Unpublished tests with CELEST1D for non-relativistic plasmas and large time steps give excellent agreement between a Darwin formulation and a fully electromagnetic formulation. It should be noted that it is possible in principle, if not in practice, to recover all time and length scales by reducing the time step and mesh spacing.

With large time steps compared with the electron gyrofrequency, electron motion across magnetic field lines is suppressed, and only motion along the field lines is allowed (Brackbill and Forslund,1985). Accurate guiding center motion is recovered with a modified particle equation of motion (Vu and Brackbill, 1995). Guiding center and gyrokinetic equations have also been used successfully (Cohen et al.,1996).

One may ask what is the contribution of kinetic electrons in the implicit solutions. Certainly, wave particle interactions on the electron plasma frequency time scale are lost. However, there is evidence the electrons contribute in important ways on the ion time scale. Electron pressure can cause thermal magnetic waves in strongly heated plasmas (Forslund and Brackbill, 1982). Electron heating appears to cause nonlinear saturation of the lower hybrid drift instability (Brackbill *et al.*,1984). Direct comparisons of hybrid (fluid electrons) and kinetic switch-off simulations with large time steps show that electrons are responsible for decay of the trailing magnetic wave (Vu and Brackbill, 1993). Comparison of hybrid and kinetic simulations of contact discontinuities show that the absence of electron thermal transport in hybrid simulations gives nonphysical results when the electron and ion temperatures are comparable (Lapenta and Brackbill,1996). Generally speaking, kinetic electrons contribute inertial effects, anisotropic pressure, and electron thermal transport on the ion time scale that would otherwise have to be modeled if fluid electron equations were used.

The implicit moment method has been applied to many problems in space plasma physics in two dimensions (Quest *et al.*, 1983; Forslund *et al.*; 1984, Dreher *et al.*, 1996; Tanaka, 1995). In three dimensions, CELESTE3D gives comparable results to those published in previous studies of the drift-kink instability (Lapenta and Brackbill, 1997) where comparisons of the simulation results with linear theory were also performed. In two dimensions, results with CELESTE3D for the tearing instability agree well with theory as described below.

The simulation domain has dimensions $12.5L \times 12.5L \times 8L$. The domain is resolved by a uniformly spaced grid with $25 \times 25 \times 64$ cells in x, y, and z respectively. (By comparison, Pritchett *et al.*, 1996 used a grid with $128 \times 128 \times 128$ cells for a somewhat larger domain.) Approximately 2.2 million particles are used to model the electrons and ions. On average, this provides 27 particles per cell per species. This number of particle per cell is adequate as second order b-spline particle assignment functions are used to reduce the noise fluctuations (Vu and Brackbill, 1992).

The computational domain is periodic in x and y. In the z direction the fields are subject to a Dirichlet boundary condition and the particles are reflected at the wall. This latter boundary condition is not particularly important, as the plasma density is small at the boundary of a Harris equilibrium.

No background plasma is used in the calculations presented below. In presence of a background, a Kelvin-Helmholtz instability may cause kinking of the current sheet similar to the drift kink instability (Kuznetsova *et al.*, 1997). However, comparisons of calculations with CELESTE3D without and with a background Maxwellian plasma of $1/10$ the peak density of the Harris equilibrium, as in (Ozaki *et al.*, 1996), yield no significant differences in the cases tested.

3 Results

Both the tearing and kink modes are 2D modes that originate from a perturbation in the y component of the vector potential:

$$A_y(x,y,z,t) = A(z)e^{i2\pi m_x x/L_x + i2\pi m_y y/L_y - i\omega t} \tag{6}$$

Modes with $m_x \neq 0$ and $m_y = 0$ are tearing modes and A_y has even parity in z; modes with $m_x = 0$ and $m_y \neq 0$ are kink modes and A_y has odd parity in z. In addition, in a 3D calculation m_x and m_y can both be different from zero (oblique modes). The primary result of the present work is to show that modes with nonvanishing m_x and m_y exist and that their parity is even, causing reconnection.

Figures 1–5 display the growth from the 3D run described above of modes corresponding to various values of (m_x, m_y) described by Eq. (6). Clearly, the linear stage of the evolution continues until $\omega_{ci}t \simeq 20$, when the drift-kink instability has grown to significant amplitude and alters the initial equilibrium enough to modify the growth rates. For comparison, Figure 6 shows the growth rate of a 2D simulation of the tearing instability alone. When the other modes are absent, the tearing mode grows with the rate predicted by the linear theory until its natural saturation is reached.

The linear growth rates can be computed from an exponential best fit of the data shown in Figs. 1–5 for $0 < \omega_{ci}t < 20$. Comparisons of the theoretical and computed values of the growth rates are summarized in Table 1. The real frequencies are $\omega_r/\omega_{ci} = 0.3$ for the drift–kink mode, and $\omega_r/\omega_{ci} = 1.4$ for the oblique mode. (The real frequencies are calculated from the time evolution of the phase of the complex amplitude of the Fourier mode.) The tearing mode is, of course, a purely growing mode ($\omega_r = 0$). The mode $m_x = 1, m_y = 0$

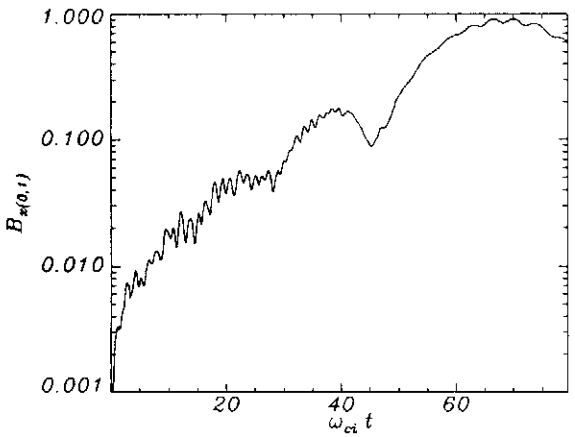

Fig. 1. Time history of the drift kink mode, $m_x = 0$, $m_y = 1$. The Fourier component of the perturbed field, B_x, is plotted against time.

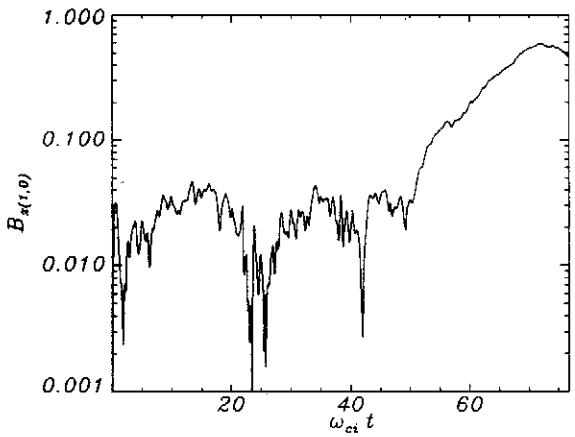

Fig. 2. Time history of the tearing mode, $m_x = 1$, $m_y = 0$. The Fourier component of the perturbed field, B_x, is plotted against time.

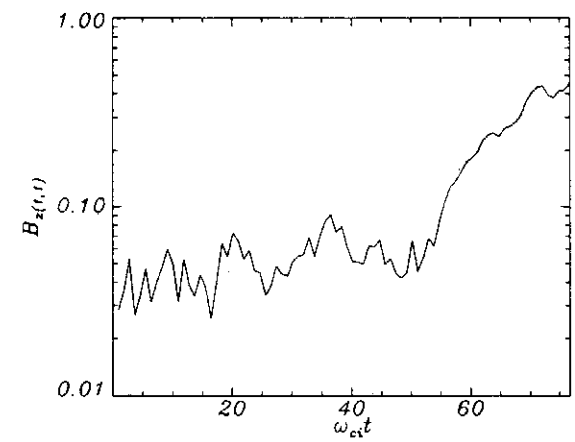

Fig. 3. Time history of the oblique mode, $m_x = 1$, $m_y = 1$. The Fourier component of the perturbed field, B_z, is plotted against time.

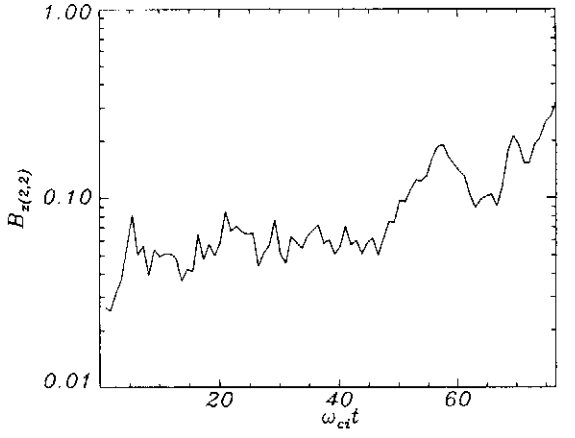

Fig. 4. Time history of the oblique mode, $m_x = 2$, $m_y = 2$. The Fourier component of the perturbed field, B_z, is plotted against time.

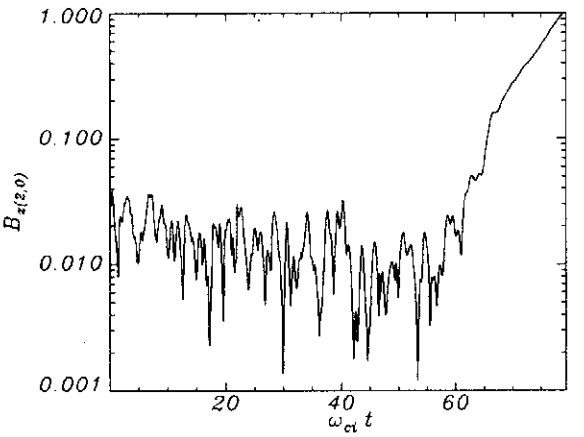

Fig. 5. Time history of the tearing mode, $m_x = 2$, $m_y = 0$. The Fourier component of the perturbed field, B_z, is plotted against time.

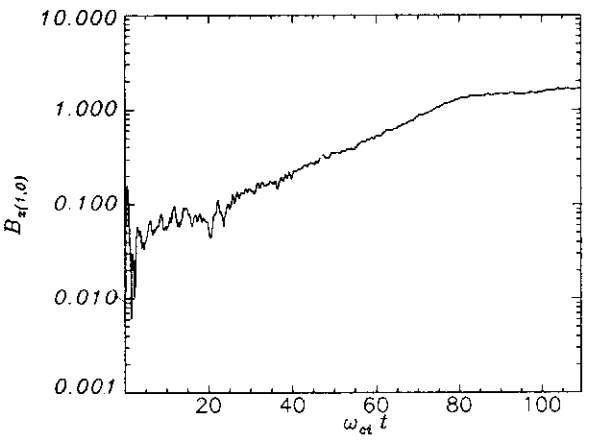

Fig. 6. Time history of the tearing mode, $m_x = 1$, $m_y = 0$ in a reference 2D calculation. The Fourier component of the perturbed field, B_z, is plotted against time.

Table 1. Growth Rates of Primary Modes. Theoretical results from Lapenta and Brackbill (1997).

MODE	Growth (linear theory)		Growth (simulation)
mass ratio m_i/m_e	16	180	180
TEARING	0.102	0.057	0.06
DRIFT KINK	0.109	0.140	0.13
OBLIQUE	N/A	N/A	0.02

is a pure tearing mode, and $m_x = 0$, $m_y = 1$ is a pure kink mode. Clearly, the growth rate of the kink mode, Fig. 1, far exceeds that of the tearing mode in three dimensions, Fig. 2. The growth rate of the oblique mode, $m_x = 1$, $m_y = 1$, is the smallest but it is above the noise of the numerical simulation. The growth rate of the fundamental oblique mode ($m_x = 1$, $m_y = 1$ see Fig. 3) exceeds that of other oblique modes $m_x = 2$, $m_y = 2$ (Fig. 4); $m_x = 1$, $m_y = 2$ and $m_x = 2$, $m_y = 1$ (not shown). Higher order modes ($m_x, m_y > 2$) are responsible for other instabilities such as the lower hybrid drift instability (see Fig. 9 below).

The parity of the oblique modes determines their effect on the initial equilibrium. It is interesting to note that a check of the computational results for the oblique mode $m_x = 1$ and $m_y = 1$ shows that A_y, Fig. 7, has even parity like the tearing mode, and thus that it can cause reconnection. By contrast, for the pure kink mode, A_y has odd parity. (The parities of various modes are summarized in Table 2).

After the initial ($0 < \omega_{ci}t < 20$) linear growth, the different modes start to interact. The drift-kink mode is the fastest and enters the non-linear stage first. The other modes are affected also, and at later times the growth is no longer monotonic. The relative level of the various modes at different stages of the non linear evolution can be observed in Figs. 1–5.

At the end of the simulation ($\Omega_{ci}t = 77$) two primary features are evident: the kink mode has produced a bending of the current sheet and the tearing and oblique modes have changed the topology of the field lines.

The first aspect is shown in Figure 8, where the contours of constant B_x are plotted. The central region of the current sheet ($-0.5 \leq z/L \leq 0.5$) has developed a kink with dominant mode number 1. At earlier stages ($\Omega_{ci}t = 22$, Fig. 9), at the edge of the current sheet a lower hybrid drift instability is visible with dominant mode number 4. Consistent with earlier results, the LHDI is localized where the density gradients are largest, does not penetrate the current sheet, and causes only minor modifications of the density profile

Table 2. Parity of Primary Modes

MODE	A_y, E_y	A_x, E_x	A_z, E_z	B_x	B_y	B_z
Tearing	even	–	–	odd	–	even
Drift-Kink	odd	–	even	even	–	–
Oblique	even	even	odd	odd	odd	even

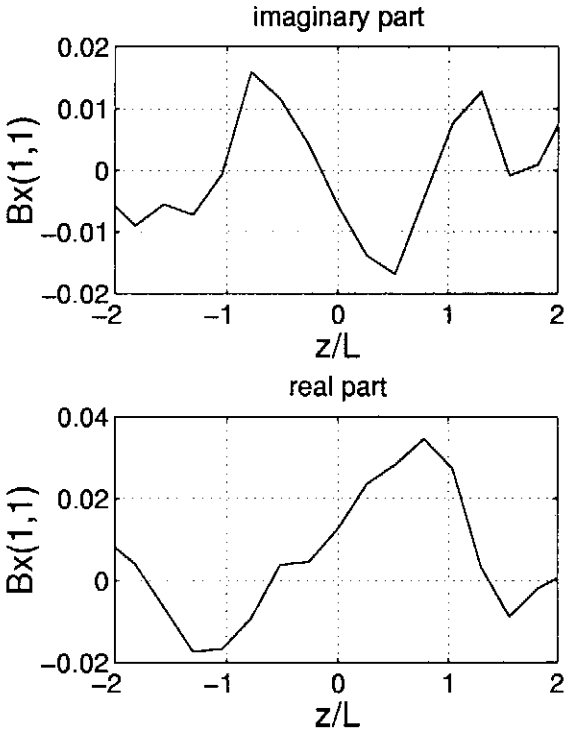

Fig. 7. In the current sheet, the $m_x = 1$, $m_y = 1$ component of B_x due to the oblique kink mode has odd parity, corresponding to even parity for A_y, Table 2, similar to the tearing mode.

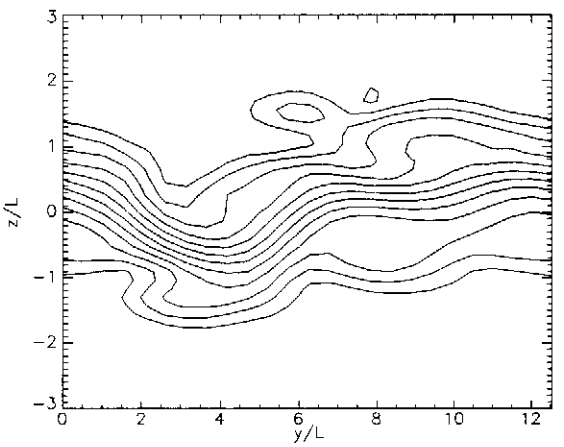

Fig. 8. Contours of constant B_x in the y, z plane are shown at the end of the simulation $\Omega_{ci}t = 77$. The drift-kink instability has reached into the non-linear phase.

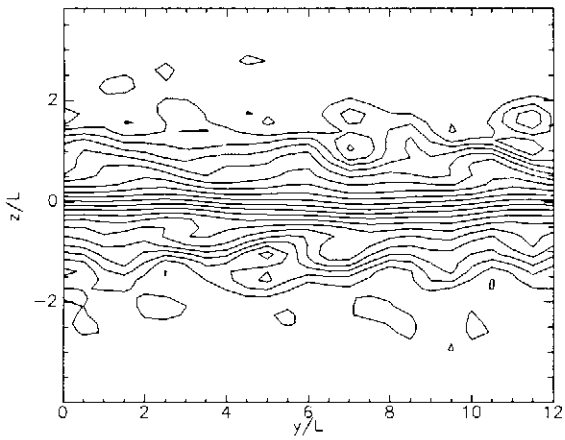

Fig. 9. Contours of constant B_x in the y, z plane are shown at $\Omega_{ci}t = 22$. The contours reflect mild kinking of the current sheet near the center of the sheet, and a lower hybrid drift instability at the edges.

(Brackbill *et al.*, 1984).

The second aspect is shown by the magnetic surfaces and magnetic field lines. In Figure 10(a and b) are plotted contours of A_y, the y component of the vector potential at $\Omega_{ci}t = 77$, with $y/L = 0$ and $y/L = 5$ (Fig. 10a and 10b, respectively). Note that the projection of $\mathbf{B}$ on to the $x - z$ plane is everywhere tangent to contours of constant A_y, i.e. the closed contours of Fig. 10 represent cross-sections of the magnetic surfaces. In 3D, closed contours of A_y may correspond to helical magnetic field lines. Note that the position of the magnetic islands is shifted between Fig. 10a and 10b. The effect is due to the kinking of the current sheet, which causes variations in the vertical shifts at different positions along y.

Figure 10 shows that higher order ($m_x = 2$) modes become relevant in the non-linear stage of the evolution (note the two-island structure). This results is confirmed further by the time histories (Figs. 4–5).

As noted by Greene (1988) and others, magnetic null points play a special role in three-dimensional reconnection. In Fig. 11 is shown one field line originating from one null point and ending in another. The null points are both spiral with one real and two complex eigenvalues. The right null is type B_S, negative real eigenvalue, and the left type A_S, positive real eigenvalue (Lau and Finn, 1990). The null-null line is traced by integrating forward and backward along the magnetic field from a selected point (dot in Fig. 11). (There is, of course, at least one more null-null line joining the two nulls because of periodicity.) In fact, the presence of field lines connecting null points is in itself a result of reconnection. While there are several examples of analytic field null solutions (Lau and Finn, 1990; Priest and Titov, 1996), Fig. 11 is the first reported result from a kinetic self-consistent plasma simulation.

The magnetic lines observed in Fig. 11 are incompatible with the pure tearing mode, where no B_y is present.

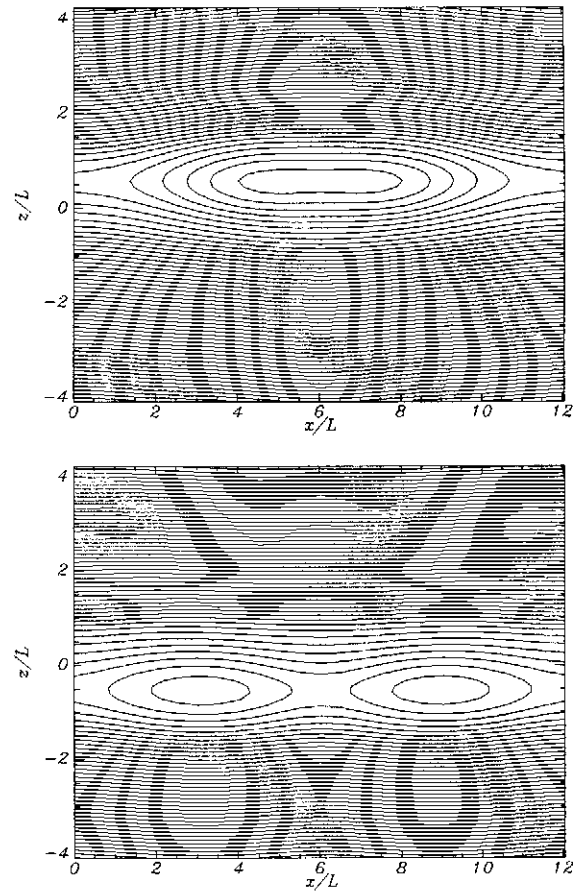

Fig. 10. Closed contours of constant A_y, the y component of the vector potential, plotted in an $x - z$ plane at $\Omega_{ci}t = 77$ reveal that reconnection has occurred. Two cross sections along y are shown: $y/L = 0$ (a- top), $y/L = 5$ (b- bottom).

However, they are consistent with oblique modes. Indeed, if $\mathbf{B} = \nabla \times \mathbf{A}$ is calculated, all three components of $\mathbf{B}$ differ from zero, yielding a $3D$ mode with the 3D helical structure suggested by the field line plots in Fig. 11.

In summary, an oblique mode is observed to grow during the linear and non-linear stage of the simulation (Fig. 3); it has the right parity to cause reconnection (Fig. 7); it forms magnetic islands with a helical structure (Fig. 11). Thus, one can reasonably argue that the oblique mode is a direct cause of reconnection in the 3D case.

4 Conclusions

We have simulated in three dimensions a system initially in a 1D Harris equilibrium using the implicit code CELESTE3D. Our simulations consider a higher mass ratio than used previously. The higher mass ratio reduces the growth rate of the tearing instability relative to the drift kink instability, thus giving a clear separation of time scales. The absence of a perpendicular magnetic field eliminates the role of electron adiabaticity in suppressing the tearing instability. Finally, the

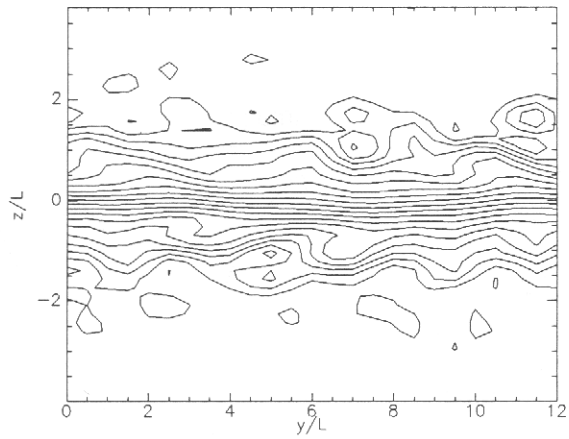

Fig. 9. Contours of constant B_x in the y, z plane are shown at $\Omega_{ci}t = 22$. The contours reflect mild kinking of the current sheet near the center of the sheet, and a lower hybrid drift instability at the edges.

(Brackbill *et al.*, 1984).

The second aspect is shown by the magnetic surfaces and magnetic field lines. In Figure 10(a and b) are plotted contours of A_y, the y component of the vector potential at $\Omega_{ci}t = 77$, with $y/L = 0$ and $y/L = 5$ (Fig. 10a and 10b, respectively). Note that the projection of $\mathbf{B}$ on to the $x - z$ plane is everywhere tangent to contours of constant A_y, i.e. the closed contours of Fig. 10 represent cross-sections of the magnetic surfaces. In 3D, closed contours of A_y may correspond to helical magnetic field lines. Note that the position of the magnetic islands is shifted between Fig. 10a and 10b. The effect is due to the kinking of the current sheet, which causes variations in the vertical shifts at different positions along y.

Figure 10 shows that higher order ($m_x = 2$) modes become relevant in the non-linear stage of the evolution (note the two-island structure). This results is confirmed further by the time histories (Figs. 4–5).

As noted by Greene (1988) and others, magnetic null points play a special role in three-dimensional reconnection. In Fig. 11 is shown one field line originating from one null point and ending in another. The null points are both spiral with one real and two complex eigenvalues. The right null is type B_S, negative real eigenvalue, and the left type A_S, positive real eigenvalue (Lau and Finn, 1990). The null-null line is traced by integrating forward and backward along the magnetic field from a selected point (dot in Fig. 11). (There is, of course, at least one more null-null line joining the two nulls because of periodicity.) In fact, the presence of field lines connecting null points is in itself a result of reconnection. While there are several examples of analytic field null solutions (Lau and Finn, 1990; Priest and Titov, 1996), Fig. 11 is the first reported result from a kinetic self-consistent plasma simulation.

The magnetic lines observed in Fig. 11 are incompatible with the pure tearing mode, where no B_y is present.

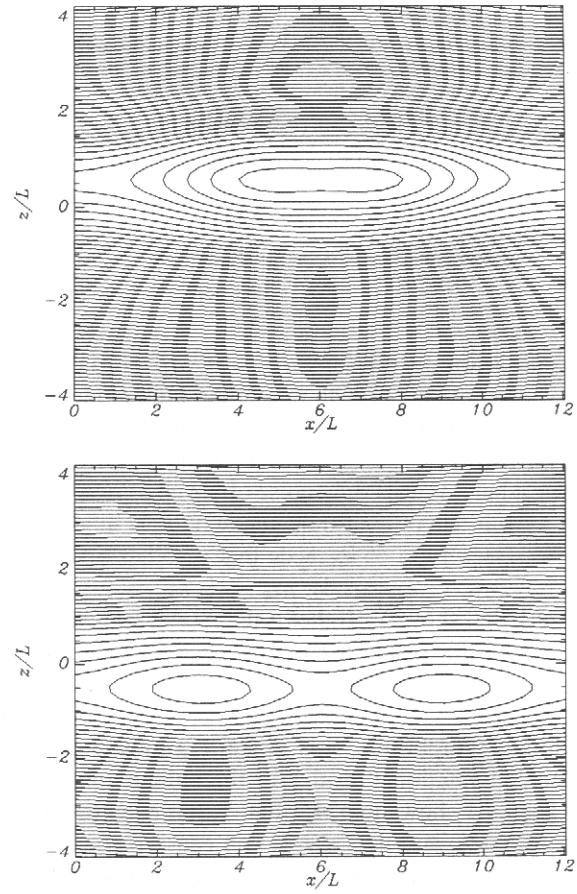

Fig. 10. Closed contours of constant A_y, the y component of the vector potential, plotted in an $x - z$ plane at $\Omega_{ci}t = 77$ reveal that reconnection has occurred. Two cross sections along y are shown: $y/L = 0$ (a- top), $y/L = 5$ (b- bottom).

However, they are consistent with oblique modes. Indeed, if $\mathbf{B} = \nabla \times \mathbf{A}$ is calculated, all three components of $\mathbf{B}$ differ from zero, yielding a $3D$ mode with the 3D helical structure suggested by the field line plots in Fig. 11.

In summary, an oblique mode is observed to grow during the linear and non-linear stage of the simulation (Fig. 3); it has the right parity to cause reconnection (Fig. 7); it forms magnetic islands with a helical structure (Fig. 11). Thus, one can reasonably argue that the oblique mode is a direct cause of reconnection in the 3D case.

4 Conclusions

We have simulated in three dimensions a system initially in a 1D Harris equilibrium using the implicit code CELESTE3D. Our simulations consider a higher mass ratio than used previously. The higher mass ratio reduces the growth rate of the tearing instability relative to the drift kink instability, thus giving a clear separation of time scales. The absence of a perpendicular magnetic field eliminates the role of electron adiabaticity in suppressing the tearing instability. Finally, the

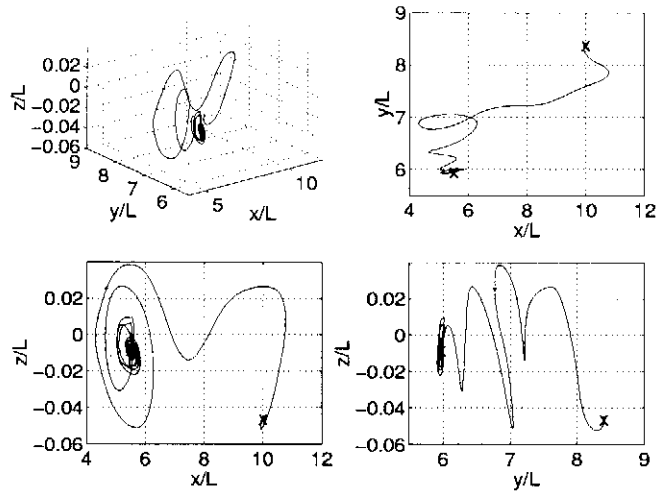

Fig. 11. A magnetic field line connecting two null points (marked with the symbol ×) is plotted at $\Omega_{ci}t = 22$. The existence of a null point that can be reached by following a field line is evidence that reconnection has occurred. The field line reflects the helical structure of the magnetic island that results from reconnection.

symmetry of the Harris equilibrium permits a clear identification of the role of each mode in reconnection.

The results of the simulations agree with the linear stability theory, with regard to the growth rate of the tearing and drift-kink instability. The results also show that the oblique kink instability, $m_x = 1$, $m_y = 1$, grows and that its parity corresponds to that of a reconnecting mode. In fact, the results show that the growth of the oblique mode is accompanied by reconnection that results in a helical magnetic structure.

The correspondence of the mode structure (parity) and relatively large amplitude of the oblique mode are evidence that the oblique mode combines properties of the drift kink and tearing instabilities. The helical structure of the reconnected field lines suggests that the oblique mode can be a direct cause of reconnection in 3D. It appears from the results presented here that the role of the drift-kink instability and of the oblique mode is not to enable more rapid growth of the pure tearing mode. Rather, the oblique mode appears directly to cause reconnection. While these simulation results apply only to the 1D Harris equilibrium, they suggest a closer examination of reconnection in a 2D, magnetotail-like equilibrium in three dimensions, especially at higher mass ratios. The results certainly provide additional motivation to examine the linear stability of the drift kink and tearing instabilities within a unified, three-dimensional analysis.

Acknowledgements. The authors wish to thank Joachim Birn, John Finn and Karl Schindler for fruitful suggestions about reconnection in 3D and magnetic field line topology. This research is supported by the Department of Energy, under contract W-7405-ENG-36, and by the NASA Sun-Earth Connection Theory Program. The Cray Supercomputer used in this investigation was provided through funding by the NASA Offices of Mission to Planet Earth, Aeronautics, and Space Science.

References

Brackbill, J. U., and D. W. Forslund, Simulation of Low-Frequency, Electromagnetic Phenomena in Plasmas, *in Multiple Time Scales*, J. U. Brackbill and B. I. Cohen Eds. (Academic Press, Orlando, 1985), pp. 271–310.

Brackbill, J. U., Plasma Simulation on Magnetohydrodynamic Time Scales, *in Proc. First International Conference on Supercomputing in Nuclear Applications, Ed. JAERI (Nuclear Energy Data Center, 1990)*, 192.

Brackbill, J. U., D. W. Forslund, K. B. Quest, and D. Winske, Nonlinear Evolution of the Lower-Hybrid Drift Instability, *Phys. Fluids, 27*, 2682–2693, 1984.

Büchner, J., J.-P. Kuska, Sausage Mode Instability of Thin Current Sheets as a Cause of Magnetospheric Substorms, *Ann. Geophys., 17*, 604–612, 1999.

Cohen, B. I., A. M. Dimits, J. J. Stimson, and D. C. Barnes, Implicit-Moment, Partially Linearized Particle Simulation of Kinetic Plasma Phenomena, *Phys. Rev. E, 53*, 2708-2716, 1996.

Daughton, W. S., Linear Stability of a Current Sheet, *J. Geophys. Res., 103*, 29429, 1998.

Dreher, J., U. Arendt, and K. Schindler, Particle Simulations of Collisionless Reconnection in Magnetotail Configuration Including Electron Dynamics, *J. Geophys. Res., 101*, 27375-27381, 1996.

Forslund, D. W., and J. U. Brackbill, Magnetic-Field Induced Surface Transport on Laser-Irradiated Foils, *Phys. Rev. Lett., 48*, 1614, 1982.

Forslund, D. W., K. B. Quest, J. U. Brackbill, and K. Lee, Collisionless Dissipation in Quasi-Perpendicular Shocks, *J. Geophys. Res, 89*, 2142-2150, 1984.

Greene, John M., Geometrical Properties of Three-Dimensional Reconnecting Magnetic Fields with Nulls, *J. Geophys. Res., 93*, 8583–8590, 1988.

Horiuchi, R. and T. Sato, Three-dimensional Simulation of Plasma Instabilities and Collisionless Reconnection in a Current Sheet, *Phys. Plasmas, 6*, 4565–4574, 1999.

Kuznetsova, M. M, M. Hesse, D. Winske, Dynamics of Drift Modes in the Magnetotail, *EOS, 78*, 625, 1997.

Lapenta, G., and J. U. Brackbill, Contact Discontinuities in Collisionless Plasmas: A Comparison of Hybrid and Kinetic Simulations, *Geophys. Res. Lett., 23*, 1713-1716, 1996.

Lapenta, G., and J. U. Brackbill, A Kinetic Theory for the Drift-Kink Instability, *J. Geophys. Res., 102*, 27099–27108, 1997.

Lapenta, G., and J. U. Brackbill, Three-Dimensional Stability of Thin Current Sheets, *EOS, 78*, 576, 1997.

Lau, Y.-T., and J. M. Finn, Three-Dimensional Kinematic Reconnection in the Presence of Field Nulls and Closed Field Lines, *Ap. J, 350*, 672–691, 1990.

Ozaki, M., T. Sato, R. Horiuchi, and Complexity Simulation Group, Electromagnetic Instability and Anomalous Resistivity in a Magnetic Neutral Sheet, *Phys. Plasmas, 3*, 2265, 1996.

Priest, E. R., and V. S. Titov, Magnetic Reconnection at Three-Dimensional Null Points, *Phil Trans. R. Soc. Lond. A, 354*, 2951-2992, 1996.

Pritchett, P. L., and F. V. Coroniti, The Role of the Drift Kink Mode in Destabilizing Thin Current Sheets, *J. Geomagn. Geoelectr., 48*, 833, 1996.

Pritchett, P. L., Collisionless Reconnection in the Magnetotail, *Adv. Space Res., 19*, 1807, 1997.

Pritchett, P. L. , F. V. Coroniti, and V. K. Decyk, Three-Dimensional Stability of Thin Quasi-Neutral Current Sheets, *J. Geophys. Res., 101*, 27413, 1996.

Quest, K. B., D. W. Forslund, J. U. Brackbill, and K. Lee, Collsionless Dissipation Processes in Quasi-Parallel Shocks, *Geophys. Res. Lett., 10*, 471-474, 1983.

Quest, K. B., H. Karimabadi, and M. Brittnacher, Consequences of Particle Conservation Along a Flux Surface for Magnetotail Tearing, *J. Geophys. Res., 101*, 179–183, 1996.

Tanaka, M., The Macro-EM Particle Simulation Method and a Study of Collisionless Magnetic Reconnection, *Comput. Phys. Commun., 87*, 117-138, 1995.

Vu, H. X., and J. U. Brackbill, CELEST1D: An Implicit, Fully Kinetic Model for Low-Frequency, Electromagnetic Plasma Simulation, *Com-*

put. Phys. Commun., 69, 253, 1992.

Vu, H. X., and J. U. Brackbill, Electron Kinetic Effects in Switch-Off Slow Shocks, *Geophys. Res. Lett. , 20*, 2015-2018, 1993.

Vu, H. X., and J. U. Brackbill, Accurate Numerical Solution of Charged Particle Motion in a Magnetic Field, *J. Comput. Phys. , 116*, 384, 1995.

Wu, C.–C., P. L. Pritchett, and F. V. Coroniti, Hydromagnetic Equilibrium and Instabilities in the Convectively Driven Near-Earth Plasma Sheet, *J. Geophys. Res., 103*, 11797–11810, 1998.

Yoon, J. H., A. T. Y. Lui, and H. K. Wong, 2-Fluid Theory of Drift-Kink Instability in a One-Dimensional Neutral Sheet, *J. Geophys. Res., 103*, 11875–11886, 1998.

Zhu, Z., and R. M. Winglee, Tearing Instability, Flux Ropes, and the Kinetic Current Sheet Kink Instability in the Earth's Magnetotail: A Three-Dimensional Perspective from Particle Simulations, *J. Geophys. Res., 101*, 4885, 1996.